

This article was downloaded by:

On: 16 January 2011

Access details: *Access Details: Free Access*

Publisher *Taylor & Francis*

Informa Ltd Registered in England and Wales Registered Number: 1072954 Registered office: Mortimer House, 37-41 Mortimer Street, London W1T 3JH, UK



## Journal of Energetic Materials

Publication details, including instructions for authors and subscription information:

<http://www.informaworld.com/smpp/title~content=t713770432>

### Shock initiation of TATB/FEFO formulations

C. M. Tarver<sup>a</sup>; D. M. Hoffman<sup>a</sup>; P. A. Urtiew<sup>a</sup>; W. C. Tao<sup>a</sup>

<sup>a</sup> Energetic Materials Center L-282 Lawrence Livermore National Laboratory, Livermore, CA

**To cite this Article** Tarver, C. M. , Hoffman, D. M. , Urtiew, P. A. and Tao, W. C.(1996) 'Shock initiation of TATB/FEFO formulations', *Journal of Energetic Materials*, 14: 3, 217 – 256

**To link to this Article:** DOI: 10.1080/07370659608216066

**URL:** <http://dx.doi.org/10.1080/07370659608216066>

PLEASE SCROLL DOWN FOR ARTICLE

Full terms and conditions of use: <http://www.informaworld.com/terms-and-conditions-of-access.pdf>

This article may be used for research, teaching and private study purposes. Any substantial or systematic reproduction, re-distribution, re-selling, loan or sub-licensing, systematic supply or distribution in any form to anyone is expressly forbidden.

The publisher does not give any warranty express or implied or make any representation that the contents will be complete or accurate or up to date. The accuracy of any instructions, formulae and drug doses should be independently verified with primary sources. The publisher shall not be liable for any loss, actions, claims, proceedings, demand or costs or damages whatsoever or howsoever caused arising directly or indirectly in connection with or arising out of the use of this material.

## SHOCK INITIATION OF TATB/FEFO FORMULATIONS

C. M. Tarver, D. M. Hoffman, P. A. Urtiew and W. C. Tao  
Energetic Materials Center L-282  
Lawrence Livermore National Laboratory  
Livermore, CA 94550

The shock initiation properties of transferable insensitive explosive (TIE) formulations based on the solid high explosive, triaminotrinitrobenzene (TATB), and the liquid explosive, bis(2-fluoro-2,2-dinitroethyl) formal (FEFO), are measured by wedge test, embedded particle velocity gauge and embedded manganin pressure gauge techniques and calculated using the Ignition and Growth reactive flow model. These extrudable formulations are demonstrated to be slightly more shock sensitive than the TATB/inert binder explosive, LX-17. However, the TIE formulations are much less sensitive than HMX-based explosives and still qualify as insensitive explosives in safety and hazard tests. The wedge tests showed a very steep dependence of run distance to detonation on the input shock pressure. Embedded gauge and reactive flow modeling results imply that shock initiation begins when a

Journal of Energetic Materials Vol 14, 217-256 (1996)  
Published in 1996 by Dowden, Brodman & Devine, Inc.

small amount of the solid TATB decomposes rapidly enough to heat the surrounding FEFO to decomposition temperature. The FEFO then reacts rapidly, raising the pressure and temperature sufficiently to cause surface decomposition of the TATB particles at rates comparable to those measured in other TATB-based explosives. An Ignition and Growth reactive flow model for TIE based on these assumptions yields reasonable agreement with the experimental shock initiation data.

### INTRODUCTION

High energy paste-extrudable explosives (PEX) based on the octahydro-1,3,5,7-tetranitro-1,3,5,7,-tetracine (HMX) molecule were developed at Lawrence Livermore National Laboratory to allow the explosive material to be stored separately from other materials and then extruded into place when needed.<sup>1</sup> These HMX-based PEX's showed reduced vulnerability to shock and impact accident scenarios relative to pressed HMX-based explosives, because they can be produced essentially void-free, thereby eliminating the mechanisms of hot spot formation and subsequent shock initiation associated with porous solid explosives.<sup>2</sup> For some applications, even greater shock insensitivity is required, and therefore PEX's based on the insensitive high explosive triaminotrinitrobenzene (TATB) were recently developed. The formulation, processing, safety testing and performance testing of these Transferable Insensitive Explosives (TIE) are discussed elsewhere.<sup>3</sup> In this

paper, the shock initiation of two TIE formulations is discussed. Like all PEX's, these two formulations contain: a solid, crystalline high explosive (TATB); an energetic liquid carrier, bis(2-fluoro-2,2-dinitroethyl) formal (FEFO); and viscosity modifiers to prevent settling. Table 1 lists the weight percentages of the ingredients present in the two TIE formations, RX-52-AD and RX-52-AE, tested in this study. The only difference is the presence of 0.55% N-100 in RX-52-AD which causes this material to cure when desired. No differences in the unreacted shock Hugoniot or the initiation properties of the cured and uncured formations were observed so they are treated as one TATB/FEFO explosive in this study. Since RX-52-AE contains 0.55% more FEFO, it has slightly more energy than RX-52-AD, as determined by cylinder test expansion,<sup>3</sup> and its reaction product equation of state is used in

TABLE 1.

PERCENT COMPOSITION OF THE TIE FORMULATIONS RX-52-

	TATB <sup>1</sup>	TATB <sup>2</sup>	FEFO	PCL <sup>3</sup>	PVF <sup>4</sup>	N-100 <sup>5</sup>
AD	47.12	17.88	31.45	1.63	1.36	0.55
AE	47.12	17.88	31.99	1.63	1.37	0.0

<sup>1</sup>Wet aminated grade TATB

<sup>2</sup>Ultrafine grade TATB

<sup>3</sup>PCL is a polycaprolactone polymer

<sup>4</sup>PVF is a polyvinyl formal polymer

<sup>5</sup>N-100 is a polyisocyanate of hexamethylene diisocyanate

this paper. Both TIE formulations accelerate metal as well as the pressed TATB-based formulation, LX-17, which contains 92.5% TATB and 7.5% Kel-F binder pressed to 98.5% of theoretical maximum density.

The shock sensitivity of the TATB/FEFO formulations was determined experimentally, and the experimental results were analyzed with the Ignition and Growth reactive flow model of shock initiation to determine the chemical energy release rates involved. The shock initiation experiments are described in the following section.

### SHOCK INITIATION EXPERIMENTS ON TIE FORMULATIONS

Three different experiments were used to determine the shock sensitivity of the TATB/FEFO formulations. The wedge test was used to measure the run distance to detonation versus input shock pressure curve (usually referred to as the "Pop Plot")<sup>4</sup> using time of arrival pins in a four inch diameter gas gun facility. The experimental geometry of this wedge test is shown in Fig. 1. The PMMA support structure was constructed with 29 time-of-arrival pins placed 2.8 mm apart and then covered with the TIE formulations. An aluminum cover plate was attached. The RX-52-AD wedges were allowed to cure. The wedges were then impacted by aluminum flyer plates at various velocities to produce different initial shock pressures and run distances to detonation. The unreacted Hugoniot equation of state of the TIE formulations was determined from

the initial shock velocities measured by the time of arrival pins and the knowledge of the aluminum equations of state. Figure 2 shows the unreacted Hugoniot states measured in the wedge and gauge tests listed in Tables 2 and 3 in pressure-particle velocity space. Also shown in Fig. 2 are the Hugoniot curves for FEFO<sup>5</sup> and LX-17<sup>6</sup> and the Jones-Wilkins-Lee (JWL) unreacted

TABLE 2.

SUMMARY OF THE WEDGE TESTS ON TIE

Flyer Vel.(mm/ $\mu$ s)	Shock Vel.(mm/ $\mu$ s)	P(GPa)	Run(mm)
1.193	3.835	5.7	>44.
1.403	4.091	7.1	33-34
1.528	4.255	7.9	22-23
1.560	4.331	8.1	21-22
1.570	4.355	8.2	20-21
1.672	4.444	9.0	16-17
1.824	4.639	10.1	10-11
1.840	4.675	10.3	9-10
2.058	4.892	12.0	3-4

TABLE 3.

EMBEDDED GAUGE EXPERIMENTS ON TIE

1. Particle Velocity Gauge Experiments (Figure 4)

Flyer Velocity(mm/ $\mu$ s)	Gauge Depths (mm)
1.372	12,17,22,26,31,36,44
1.476	0,11,16,21,26,30,35,44
1.505	0,12,17,21,26,31,36,44

2. Manganin Pressure Gauge Experiments (Figure 5)

Flyer Velocity(mm/ $\mu$ s)	Gauge Depths (mm)
1.51	13,16,19,22,25
1.53	17,20,23,26,29,32
1.60	16,19,22,24,27,30

equation of state developed for TIE shock initiation reactive flow modeling. The transitions to detonation were observed as sudden increases in shock velocity to velocities close to the measured detonation velocity. There were essentially no shock velocity increases before the transitions occurred, indicating that very little reaction occurred near the leading shocks causing them to accelerate. Liquid explosives show this type of shock front velocity behavior, whereas some solid explosives, including TATB, show significant increases in shock velocity before the transition to detonation occurs.<sup>7</sup> The run distances to detonation for the TIE wedge tests are listed in Table 2 and are plotted versus input shock pressure as a Pop Plot in Fig. 3. Also plotted in Fig. 3 are the LX-17 Pop Plot<sup>6</sup> and two run distances to detonation for pure FEFO measured by Simpson et al.<sup>5</sup> The lowest aluminum flyer plate velocity test in Table 2 failed to detonate in the 44 mm thick TIE sample, and thus the run distance is >44 mm. In Fig. 3, the TIE formulations are shown to be slightly more sensitive than LX-17 and to have a very steep Pop Plot, which is also similar to those of liquid explosives. This slightly greater shock sensitivity of TIE compared to LX-17 was confirmed by a series of electric gun experiments in which 0.25 mm thick mylar flyers impacted TIE cylinders velocities ranging from 2.6 to 4 km/s. The threshold mylar flyer velocity range for initiation of detonation in TIE formulations was 3 - 3.3 km/s. For the same mylar thickness,

the threshold velocity range for LX-17 initiation is 4.2 - 4.6 km/s.

However, the TIE formulations are still quite insensitive relative to HMX-based explosives. The threshold velocity for PBX 9404 initiation by 0.25 mm thick mylar flyers is 2.4 km/s, and comparison with the Pop Plot for PBX 9404<sup>6</sup> in Fig. 3 shows that TIE is less sensitive than HMX-based explosives. The steepness of the TIE Pop Plot indicates that it requires very long run distances to detonate at initial pressures below 5 GPa. Therefore TIE behaves similarly to other TATB-based insensitive high explosives in safety and handling tests. At extremely high pressures, the TIE Pop Plot most likely will be controlled by the FEFO component, because the FEFO will promptly shock initiate under those conditions.

To measure the chemical energy release rates of TIE during shock initiation, two other types of experiments were performed in the four inch gas gun facility. Figure 4 shows the experimental geometry of the embedded particle velocity gauge shots. Since the particle velocity gauges work on the principle of a moving electrical conductor in a magnetic field,<sup>8</sup> the TIE holder had to be built entirely of non-metallic materials (PMMA and Lexan). The flyer also had to be nonmetallic (Ceramic AD998, as used in previous LX-17 studies).<sup>9</sup> Sets of six particle velocity gauges were stretched across the holder at an angle of 36° so that the gauges, 8 mm



apart on the diagonal, were 4.7 mm apart in the axial flow direction. Two single element particle velocity gauges were also used, one placed between the Lexan buffer plate and one of the lexan side pieces to record the input pulse and the other one placed inside the PMMA bottom support to record the TIE-PMMA interface velocity. The holder was filled with TIE and allowed to cure if RX-52-AD was used. Table 3 lists the three successful particle velocity gauge shots in order of increasing AD998 flyer velocity, and the individual particle gauge records are compared to hydrodynamic calculations in a later section. The experiments were fired in the rather narrow range of flyer velocities that result in run distances to detonation where the gauges are positioned. The gauges recorded peak particle velocities consistent with detonation at run distances to detonation predicted from the wedge test results.

The third shock initiation experiment on TIE was another embedded gauge test using manganin pressure gauges. Figure 5 shows the experimental geometry, which was very similar to that used for the particle velocity gauges. Since manganin gauges measure resistance as a function of pressure, metals do not interfere with the gauge function and can be used in this experiment. The six manganin gauge elements were 5 mm apart on the 36° holder so that their spacing was 2.9 mm in the axial flow direction. No front or back surface gauges were used in these shots. Table 3 lists the three successful manganin

gauge experiments according to aluminum flyer velocity. The individual gauge records are discussed in comparison with hydrodynamic calculations in a later section. The run distances to detonation in the manganin gauge experiments were consistent with those measured in the wedge tests and particle velocity gauge shots.

### IGNITION AND GROWTH REACTIVE FLOW MODELING

The ignition and growth reactive flow of shock initiation and detonation of solid explosives has been incorporated into several hydrodynamic computer codes and used to solve many explosive and propellant safety and performance problems.<sup>9-17</sup> This model uses two Jones-Wilkins-Lee (JWL) equations of state, one for the unreacted explosive and another one for its reaction products, in the temperature dependent form:

$$p = A e^{-R_1 V} + B e^{-R_2 V} + \omega C_V T/V \quad (1)$$

where  $p$  is pressure in Megabars,  $V$  is the relative volume,  $T$  is temperature,  $\omega$  is the Gruneisen coefficient,  $C_V$  is the average heat capacity, and  $A$ ,  $B$ ,  $R_1$ , and  $R_2$  are constants. The reaction rate law for the conversion of explosive to products is:

$$\frac{dF}{dt} = I(1-F)^b(\rho/\rho_0-1-a)^x + G_1(1-F)^c F^d p^y + G_2(1-F)^e F^g p^z \quad (2)$$

$0 < F < F_{igmax} \qquad 0 < F < F_{G1max} \qquad F_{G2min} < F < 1$

where  $F$  is the fraction reacted,  $t$  is time,  $\rho$  is the current density.  $\rho_0$  is the initial density,  $p$  is pressure in Mbars, and  $I$ ,

$G_1$ ,  $G_2$ ,  $a$ ,  $b$ ,  $c$ ,  $d$ ,  $e$ ,  $g$ ,  $x$ ,  $y$ , and  $z$  are constants. As explained more fully in previous papers, this three term rate law models the three stages of reaction generally observed in shock initiation of heterogeneous solid explosives. The first term ignites some of the solid explosive as it is compressed by a shock or compression wave creating heated areas (hot spots) as the voids in the material collapse. Generally the amount of explosive ignited by a strong shock wave is approximately equal to the original void volume.<sup>2</sup> The second term in equation (2) represents the growth of reaction from the hot spots into the remaining solid. During shock initiation, this term models the relatively slow spreading of reaction in a deflagration-type process of inward or outward grain burning with pressure exponents close to one ( $y=1$  in equation (2)). The exponents of the fraction reacted terms in Eq. (2) are generally set equal to  $2/3$  to represent the surface to volume ratio for spherical particles. The third term in equation (2) describes the rapid transition to detonation observed when the growing hot spots begin to coalesce and transfer large amounts of heat to the remaining unreacted explosive particles.

The shock initiation of homogeneous liquid explosives has long been known to be quite different from that of heterogeneous solid explosives.<sup>18</sup> In liquids, the initial shock front uniformly heats the explosive to a temperature which may or may not be sufficient to cause thermal explosion at the

rear boundary of the charge (or very close to this boundary). If thermal explosion does occur after a time delay determined by the Arrhenius kinetics of the liquid, a "superdetonation" wave is created which propagates through the precompressed liquid explosive until it overtakes the initial shock wave. The resulting detonation wave then decreases in velocity until Chapman-Jouguet (CJ) steady state detonation is attained. Simpson et al.<sup>5</sup> obtained two shock initiations in pure FEFO at pressures exceeding 13 GPa and related these initiation conditions to those of other liquid explosives.<sup>19</sup> Liquid explosives are known to be sensitized by bubbles or microballoons, which create hot spots upon void collapse,<sup>20</sup> and by the addition of solid particles to create density discontinuities and turbulent heating.<sup>21</sup>

The situation is different from both these cases in the TIE formulations. They are essentially void-free or at least contain very few voids that are too small to be effective hot spot sites upon collapse. Therefore they are not subject to the mechanisms that initiate solid explosives. The liquid FEFO component surrounds the well-packed bimodal distribution of TATB particles and thus is not representative of a liquid explosive system. The most likely scenario for TIE shock initiation is that, at approximately 5.5 GPa, a small amount of TATB begins to react at collapsed internal voids and cracks and at TATB particle interfaces. One-dimensional infrared

radiometry experiments<sup>22</sup> have shown some decomposition of LX-17 at this shock pressure, but the reaction fails to grow before the hot spots cool by thermal diffusion. Pressures of 6.5 to 7 GPa are required for growth of reaction in LX-17.<sup>23</sup> In TIE, however, this localized TATB decomposition may be sufficient to heat a small volume of FEFO to thermal decomposition. If this volume of reacting FEFO is large and hot enough, it will continue to propagate, rapidly consuming the FEFO component. Then the final stage of the initiation process is high pressure, high temperature decomposition of the TATB particles which are surrounded by hot FEFO reaction products.

The Ignition and Growth reactive flow model for TIE shock initiation is based on this mechanism. At shock pressures exceeding 5.5 GPa or relative compressions exceeding 0.23 (parameter  $a$  in Eq.(2)), one percent of the explosive is assumed to react at the usual TATB ignition rate<sup>14</sup> given by the first term in Eq. (2) using the parameters listed in Table 4. The second term in Eq. (2) is then used to model the FEFO reaction by rapidly releasing 40% of the total explosive energy with a high pressure exponent ( $\gamma=4$ ). The third term in Eq. (2) then models the TATB particle decomposition releasing the final 60% of the energy release at the usual high pressure reaction completion rates for TATB.<sup>14</sup> The equation of state and reaction rate parameters for the TIE Ignition and Growth

calculations are listed in Table 4. Table 5 contains all of the Gruneisen equations of state for the inert materials used in the

TABLE 4.

REACTIVE FLOW PARAMETERS FOR TATB/FEFO

Initial Temperature = 298K	$\rho_0 = 1.78 \text{ g/cm}^3$
Detonation Velocity = 7.59 mm/ $\mu$ s	CJ Pressure = 26 GPa
<b>UNREACTED JWL</b>	<b>PRODUCT JWL    REACTION RATES</b>
A=4.0e+5 Mbar	A=6.452346 Mbar    I=4.0e+7
B=-0.0550389 Mbar	B=0.107208 Mbar    a=0.23
R <sub>1</sub> =20.0	R <sub>1</sub> =4.60    b=0.667
R <sub>2</sub> =2.00	R <sub>2</sub> =1.21    x=7.0
$\omega$ =0.8938	$\omega$ =0.35    G <sub>1</sub> =6300
C <sub>v</sub> =2.487e-5 Mbar/K	C <sub>v</sub> =1.0e-5 Mbar/K    y=4.0
T <sub>0</sub> =298 K	E <sub>0</sub> =0.066 Mbar    c=0.667
Shear Modulus=0.0354Mbar	d=0.667
Yield Strength=0.002 Mbar	G <sub>2</sub> =400
	e=0.333
	g=1.0
	z=3.0
	Fig <sub>max</sub> =0.01
	FG <sub>1max</sub> =0.4
	FG <sub>2min</sub> =0.4

TABLE 5.

GRUNEISEN EOS PARAMETERS FOR INERT MATERIALS

$$p = \rho_0 c^2 \mu [1 + (1 - \gamma_0/2)\mu - a/2\mu^2] / [1 - (S_1 - 1)\mu - S_2\mu^2 / (\mu + 1) - S_3\mu^3 / (\mu + 1)^2]^2 + (\gamma_0 + a\mu)E \quad [\mu = \rho/\rho_0 - 1 \text{ and } E \text{ is thermal energy}]$$

INERT	$\rho_0(\text{g/cm}^3)$	c(mm/ $\mu$ s)	S <sub>1</sub>	S <sub>2</sub>	S <sub>3</sub>	$\gamma_0$	a
Al 6061	2.703	5.24	1.4	0.0	0.0	1.97	0.48
Al 2024	2.785	5.37	1.29	0.0	0.0	1.97	0.48
AD998	3.998	7.916	1.90-1.95	0.0	0.0	2.0	0.0
Lexan	1.193	2.18	1.78	0.0	0.0	0.61	0.0
PMMA	1.182	2.18	2.09	-1.12	0.0	0.85	0.0

calculations. Comparisons with the experimental results are shown in the next section.

### COMPARISON OF EXPERIMENTS AND CALCULATIONS

The calculated unreacted Hugoniot curve for TIE is compared to the initial shock states measured in the wedge test in Fig. 2, and the calculated Pop Plot is compared to experiment in Fig. 3. The TIE unreacted equation of state is intermediate between the TATB and FEFO equations of state, as shown in Fig. 2. The absence of shock front growth in the wedge test measurements indicates that only a small amount of explosive is ignited by the first term in the reaction rate law. The high pressure dependence and rapid reaction rate for FEFO decomposition in the second term of the reaction rate law is needed to match the steepness and pressure regime of the TIE Pop Plot. Therefore the Ignition and Growth model accurately represents all of the experimental data that can be obtained from the wedge tests.

The two embedded gauge techniques, particle velocity and manganin pressure, yield time resolved data on the buildup of momentum (particle velocity) and pressure as chemical decomposition occurs behind the leading shock front. Three successful four inch gas gun shots were fired with each type of embedded gauge. Each experiment was calculated using the TIE Ignition and Growth reactive flow model described above. Figure 6 shows the records from the lowest

flyer velocity experiment containing embedded particle velocity gauges and the corresponding calculations. At this AD998 flyer velocity (1.372 mm/ $\mu$ s), the run distance to detonation in TIE should exceed the 44 mm sample thickness, and neither the gauges nor the calculations reach detonation conditions. The particle velocity gauges measured increasing velocities at the shock front and for a microsecond or two behind the front on the first four gauges. The calculations also showed these increases, but the growth of reaction behind the shock front was delayed by the rarefaction coming from the rear of the AD998 flyer. In this low compression regime, there is some uncertainty in the AD998 equation of state and material properties, which were addressed by Urtiew et al.,<sup>9</sup> and the calculated shock velocity in AD998 using the equation of state in Table 5 may be high, resulting in the rear rarefaction wave entering the TIE earlier than it does experimentally. Nevertheless, the overall amount of energy release calculated by the model is approximately correct, because the peak particle velocities agree with the gauge records. The gauge record and the calculation at the 44 mm gauge position on the TIE-PMMA interface indicate that detonation is nearly attained there. The particle velocities are higher at this gauge than for those embedded in TIE due to the low impedance of PMMA relative to TIE.



Figure 7 shows the results for an experiment in which the AD998 flyer velocity was 1.476 mm/ $\mu$ s. At this input pressure, detonation should occur between the gauges at 16 mm and 21 mm, as it does in both the gauge records and calculations. The calculated peak velocities are higher than those on all of the gauges. The calculated von Neumann spike particle velocity on the unreacted TIE Hugoniot is 2.2 mm/ $\mu$ s, and generally the spike states predicted for TATB-based explosives are quite accurate, because the unreacted Hugoniot can be determined to high shock pressures due to the insensitivity of TATB. The particle velocity gauge records in TIE are not as sharp as usual, especially at detonation, exhibiting much longer rise times, lower peaks and more rapid signal decays. One possible explanation for this behavior is that the filling of the sample holder with TIE slightly perturbed the orientation of the gauge package. The gauges did record detonation waves arriving at the correct times.

Figure 8 shows the results for a slightly higher flyer velocity of 1.505 mm/ $\mu$ s. Under this shock loading, detonation should occur just prior to reaching the gauge at 17 mm. The calculation for the 17 mm position predicts detonation, while the particle velocity gauge shows that the leading shock has not quite been overtaken by the reactive flow behind it and detonation has not yet been established. As in Fig. 7, the particle velocity gauges in the detonation flow have longer rise

times, lower peak values, and drop off faster than usual. The single element gauge at the TIE-PMMA interface agrees closely with the calculated particle velocity at this boundary.

The lowest pressure embedded manganin pressure gauge experiment used an aluminum flyer impacting at 1.51 mm/ $\mu$ s. The predicted run distance to detonation is approximately 25 mm. Figure 9 shows the experimental and calculated pressure histories at five gauge positions. The first gauge at 10 mm do not give a usable signal. The gauges and calculations both show a detonation wave at the 25 mm positions. The calculated growth of the shock front pressure agrees very well with the gauge records. The growth of reaction behind the shock front appears to be slow at the 13 mm and 16 mm gauges but quite close at 19 mm and 22 mm gauges. The most obvious disagreement between the gauge records and calculations is that the gauges recorded very high peak pressures at the completion of shock induced reaction and at detonation. Based on the TIE unreacted and product equations of state, which are both fit to experimental data, and those of other TATB-based explosives, such high pressures are not possible in normal one-dimensional flow.

The same trend is shown in Fig. 10, which contains the results for an experiment with an aluminum flyer velocity of 1.53 mm/ $\mu$ s, and Fig. 11, which has results for an aluminum flyer velocity of 1.60 mm/ $\mu$ s. The calculated run distances to

detonation, 23 mm in Fig. 10 and 20 mm in Fig. 11, agree with the wedge test results and the particle velocity gauge records. However, several calculated peak pressures are much lower than the measured pressures.

When these abnormally high pressures were first observed, it was thought that perhaps a thermal explosion of the liquid FEFO component occurred behind the leading shock front creating a "partial superdetonation" wave in the precompressed TIE which caused the remaining TATB to react rapidly and produce these extremely high pressures. The 17 mm deep gauge record in Fig. 10 certainly could be interpreted as a thermal explosion about  $0.5 \mu\text{s}$  after the passage of the 9 GPa shock, which drives the pressure to 30 GPa and causes further reaction for the next  $1.5 \mu\text{s}$ . To investigate the possibility of "partial superdetonation," several Ignition and Growth models using various assumptions about the FEFO and TATB reaction rates were used to calculate the hydrodynamics measured by the manganin gauge records. When partial superdetonations were produced in the calculations, they could not match all of the pressures and times of arrival at the gauge positions. They also could not decay toward the von Neumann spike pressure fast enough to agree with the lower peak pressures observed at the deepest gauge positions, such as the 32 mm gauge in Fig.10 and the 30 mm gauge in Fig. 11.

The explanation for the high measured pressures came from detailed two-dimensional modeling of the entire experimental setups shown in Figs. 4 and 5. The TIE holder for the manganin gauge shots was mostly aluminum, which has a higher shock velocity than the explosive. The embedded gauges were thought to be far enough for the aluminum parts that the shock front in the TIE would have sufficient time to cause detonation before the shock wave in the aluminum would interfere with the reactive flow. However, the small piece of aluminum holding the manganin gauge package in place, shown in the upper left hand corner in Fig. 5 just below the aluminum buffer plate, extends an additional 6 mm into the TIE explosive. When this protruding aluminum part is included in the two-dimensional calculations, it clearly creates a second shock front propagating at a different angle than the gauge package toward the axis of the explosive charge. This second shock definitely affects the reaction rates behind the leading shock front at some gauge positions and then collides at the charge axis with its counterpart from the opposite side. This causes the very high pressures measured by gauges near the charge axis. Figures 12 - 16 show the pressure contours in Megabar units for the aluminum and TIE for the manganin gauge experiment with an aluminum flyer velocity of 1.51 km/s at 3, 4, 5, 6, and 7  $\mu$ s, respectively. The shock wave in the aluminum charge holder is observed to be propagating

Downloaded At: 13:56 16 January 2011

faster than the initial shock in the TIE material and creates a second shock in the TIE at the interface. This second shock causes further reaction in the decomposing TIE, and the resulting maximum pressure contour in the TIE is growing and propagating toward the charge axis in Figs. 12 and 13. In Fig. 14, this maximum pressure reaches the charge axis and is reflected to a pressure of 38.2 GPa, close to the 40 GPa pressure measured by the manganin gauges. This high pressure region propagates along the charge axis in Figs. 15 and 16. Gauges in its path record pressures approaching 40 GPa. Some gauges deeper into the explosive and not near the charge axis, such as the deepest gauges in Figs. 10 and 11, were not affected and recorded normal detonation pressures.

The embedded particle velocity gauges were not affected by this phenomena, because the nonmetallic materials PMMA and Lucite were used to construct the TIE charge holders. These materials have lower shock velocities than TIE, and detailed two-dimensional hydrodynamic calculations showed that no shocks from the PMMA or Lexan parts could perturb the reactive flow in the TIE, which showed maximum rates of reaction at its charge axis.

#### SUMMARY AND CONCLUSIONS

The shock initiation of cured and uncured TIE formulations based on TATB in a liquid FEFO matrix was studied using wedge tests, thin mylar flyer from an electric

gun, embedded particle velocity gauges and embedded manganin pressure gauges. These TIE formulations were demonstrated to be slightly more sensitive than LX-17 but still are within the general classification of insensitive high explosives. Therefore these TIE formulations should be very useful in applications where the explosive is required to be stored separately from the rest of the materials and an insensitive high explosive is required once the explosive is formed into its final shape. An Ignition and Growth reactive flow model for TIE was developed by assuming that, above a certain shock pressure, a small but sufficient amount of TATB reacts causing the surrounding FEFO to rapidly react, which in turn causes high pressure, high temperature surface decomposition of the remaining TATB particles. This model agrees with the run distance to detonation and embedded gauge data. Some spurious high pressure measurements were traced to secondary shock fronts in the TIE created by the geometry of and materials present in the experiment. The experiments can easily be redesigned to avoid multiple shock effects.

#### ACKNOWLEDGEMENTS

This work was performed under the auspices of the United States Department of Energy by the Lawrence Livermore National Laboratory under Contract No. W-7405-ENG-48. The authors would like to thank Connie Walkup and

Leslie Spellman for formulating the TIE materials, Richard Simpson for small scale testing, Frank Garcia for supervising the gas gun shots, and P. Clark Souers for the product JWL equation of state.

#### REFERENCES

1. E. von Holtz, K. J. Scribner, R. Whipple and J. Carley, Paste-Extrudable Explosives and their Current Status, Lawrence Livermore National Laboratory, UCRL-JC-103244 (1990).
2. E. L. Lee and C. M. Tarver, Phys. Fluids 23, 2362 (1980).
3. D. M. Hoffman, C. M. Walkup, L. Spellman and W. C. Tao, Transferable Insensitive Explosives (TIE), Lawrence Livermore National Laboratory Report, in press.
4. J. B. Ramsay and A. Popolato, Fourth Symposium (International) on Detonation, Office of Naval Research ACR-126, White Oak, MD, 1965, p. 233.
5. R. L. Simpson, F. H. Helm and E. H. von Holtz, Shock Compression and Initiation Behavior of FEFO, Lawrence Livermore National Laboratory Report UCID-21575, November, 1988.
6. B. M. Dobratz, LLNL Explosives Handbook, Lawrence Livermore National Laboratory Report UCRL-52997, March, 1981.
7. A. B. Anderson, M. J. Ginsberg, W. L. Seitz and J. Wackerle, Seventh Symposium (International) on Detonation, Naval

Surface Weapons Center NSWC MP 82-334, Annapolis, MD, 1981, p. 385.

8. L. M. Erickson, C. B. Johnson, N. L. Parker, H. C. Vantine, R. C. Weingart and R. S. Lee, Seventh Symposium (International) on Detonation, Naval Surface Weapons Center NSWC MP 82-334, Annapolis, MD, 1981, p. 1062.

9. P. A. Urtiew, L. M. Erickson, D. F. Aldis and C. M. Tarver, Ninth Symposium (International) on Detonation, Office of the Chief of Naval Research OCNR 113291-7, Portland, OR, 1989, p. 112.

10. C. M. Tarver and L. G. Green, Ninth Symposium (International) on Detonation, Office of the Chief of Naval Research OCNR 113291-7, Portland, Oregon, 1989, p. 701.

11. C. M. Tarver and J. O. Hallquist, Seventh Symposium (International) on Detonation, Naval Surface Weapons Center NSWC MP 82-334, Annapolis, MD, 1981, p.488.

12. C. M. Tarver, N. L. Parker, H. G. Palmer, B. Hayes and L. M. Erickson, *J. Energetic Materials* 1, 213 (1983).  
*Phys.* 80, 3831 (1984).

14. C. M. Tarver, J. O. Hallquist and L. M. Erickson, Eighth Symposium (International) on Detonation, Naval Surface Weapons Center NSWC 86-194, Albuquerque, NM, 1985, p. 951.

15. C. M. Tarver, *Propellants, Explosives and Pyrotechnics* 15, 132 (1990).



16. C. M. Tarver, P. A. Urtiew, S. K. Chidester and L. G. Green, *Propellants, Explosives and Pyrotechnics* 18, 117 (1993).
17. C. M. Tarver, T. M. Cook, P. A. Urtiew and W. C. Tao, *Multiple Shock Initiation of LX-17*, Proceedings of the Tenth Symposium (International) on Detonation, Boston, MA, 1993, in press.
18. A. W. Campbell, W. C. Davis and J. R. Travis, *Phys. Fluids* 4, 498 (1961).
19. C. M. Tarver, R. Shaw and M. Cowperthwaite, *J. Chem. Phys.* 64, 2665 (1976).
20. V. K. Mohan and J. E. Hay, *Seventh Symposium (International) on Detonation*, Naval Surface Weapons Center NSWC MP 82-334, Annapolis, MD, 1981, p. 373.
21. S. A. Sheffield, R. Engelke and R. R. Alcon, *Ninth Symposium (International) on Detonation*, Office of the Chief of Naval Research OCNR 113291-7, Portland, OR, 1989, p. 39.
22. W. G. Von Holle, *Shock Waves in Condensed Matter-1983*, J. R. Asay, R. A. Graham and G. K. Straub, eds., North-Holland, New York, 1984, p. 283.
23. K. Bahl, G. Bloom, L. Erickson, R. Lee, C. Tarver, W. Von Holle and R. Weingart, *Eighth Symposium (International) on Detonation*, Naval Surface Weapons Center NSWC MP 86-194, Albuquerque, NM, 1985, p. 1045.

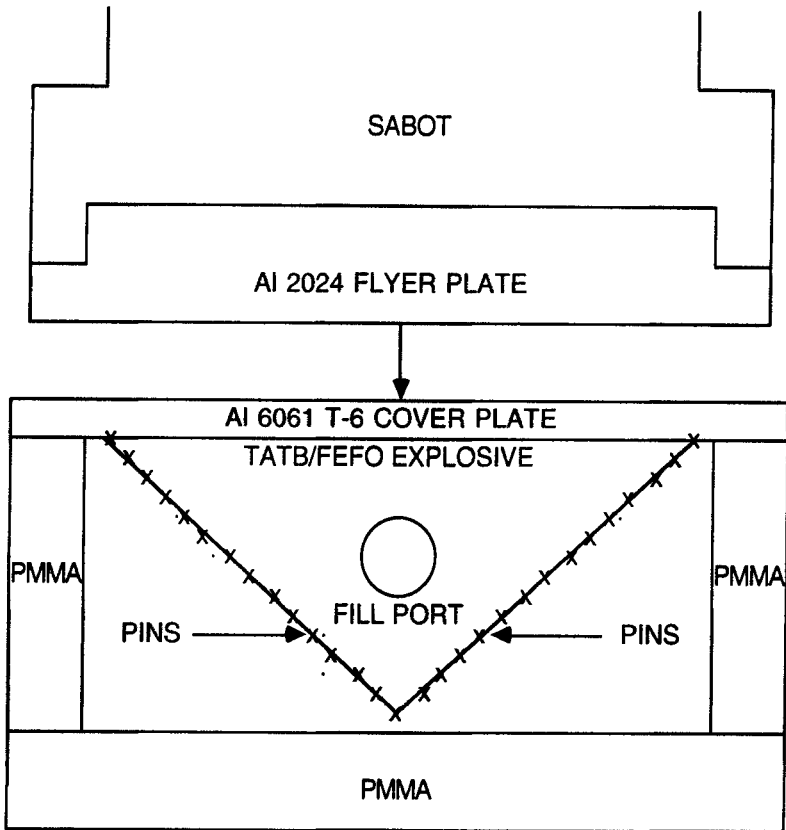


FIGURE 1  
Experimental Geometry for TIE Wedge Tests

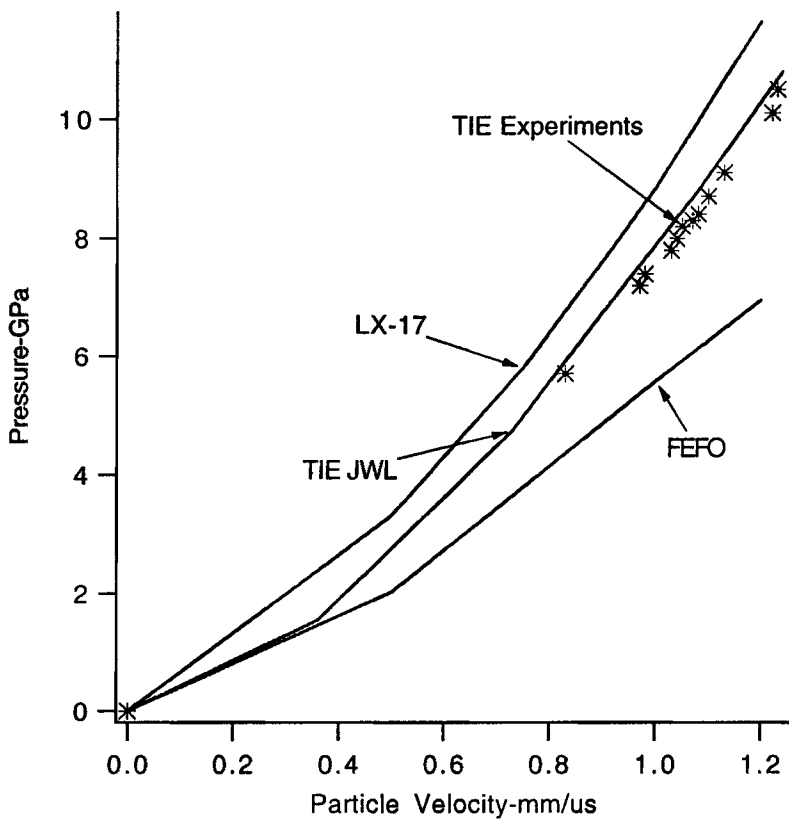


Figure 2. Pressure versus Particle Velocity States on the Unreacted Explosive Hugoniot

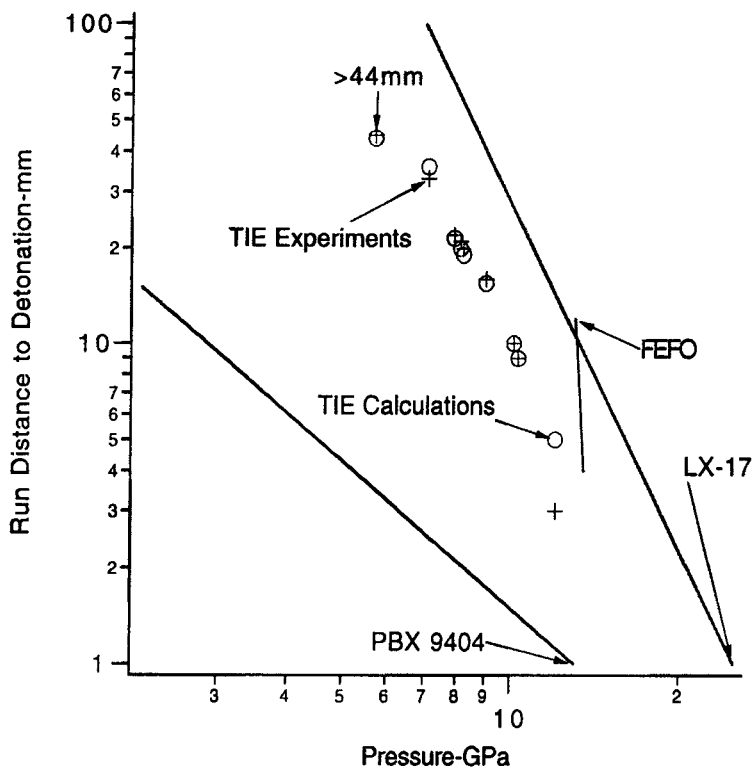


Figure 3. Run Distance to Detonation versus Input Shock Pressure for TIE, LX-17, FEFO, and PBX 9404

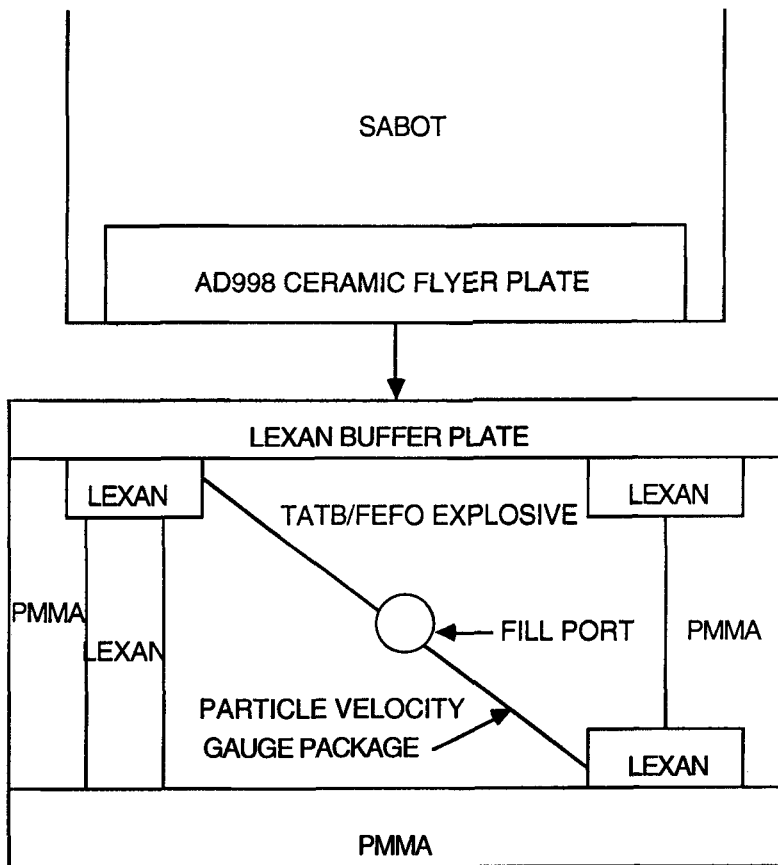


FIGURE 4

Experimental Geometry for Particle Velocity Gauge Shots

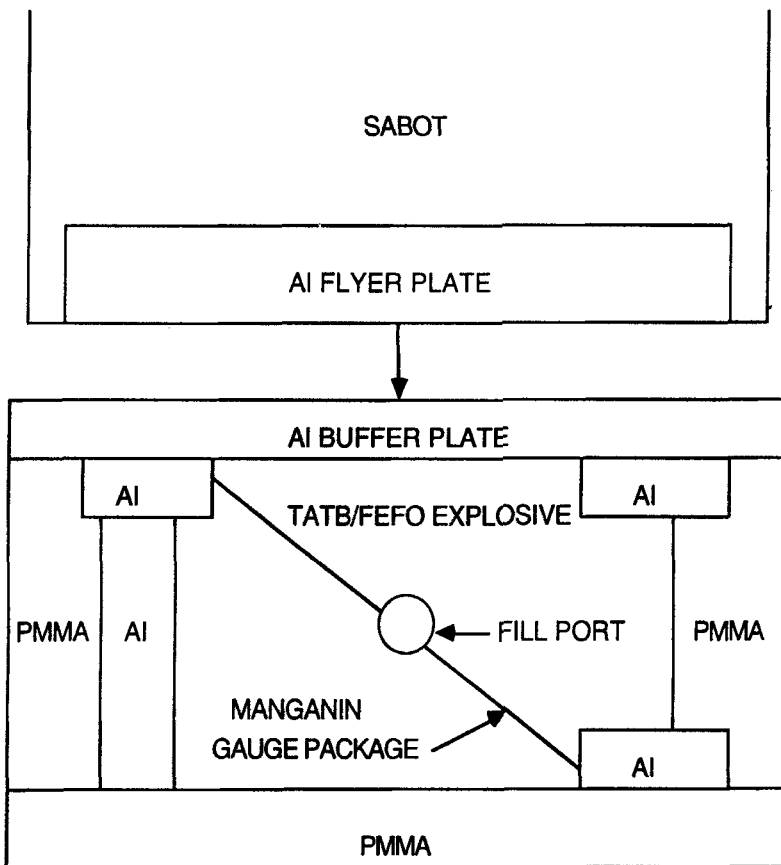


FIGURE 5  
Experimental Geometry for Manganin Pressure Gauge Shots

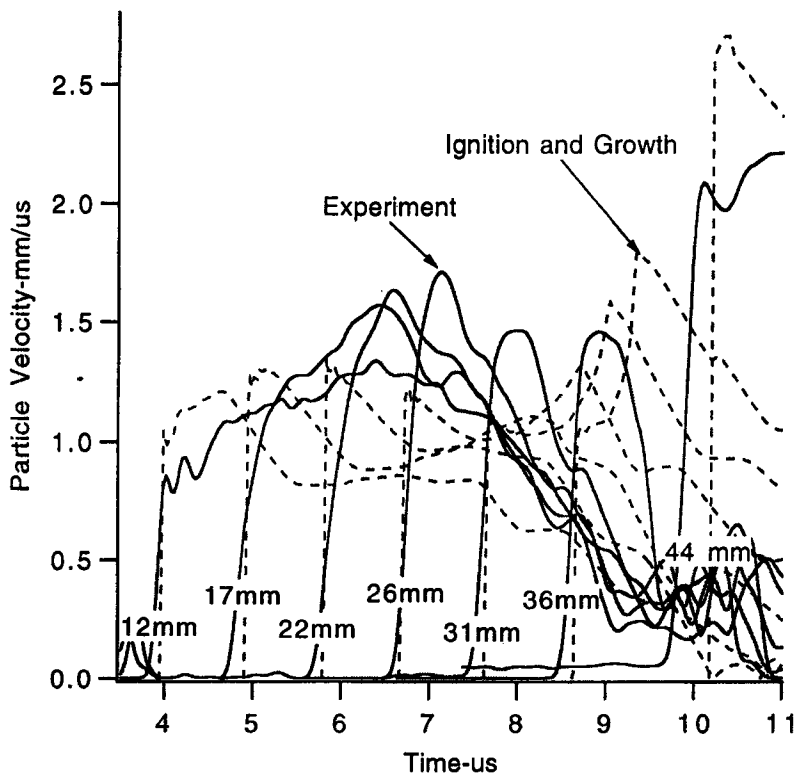


Figure 6. Experimental and Calculated Particle Velocity Histories in TATB/FEFO Impacted by an AD998 Flyer at 1.372 km/s

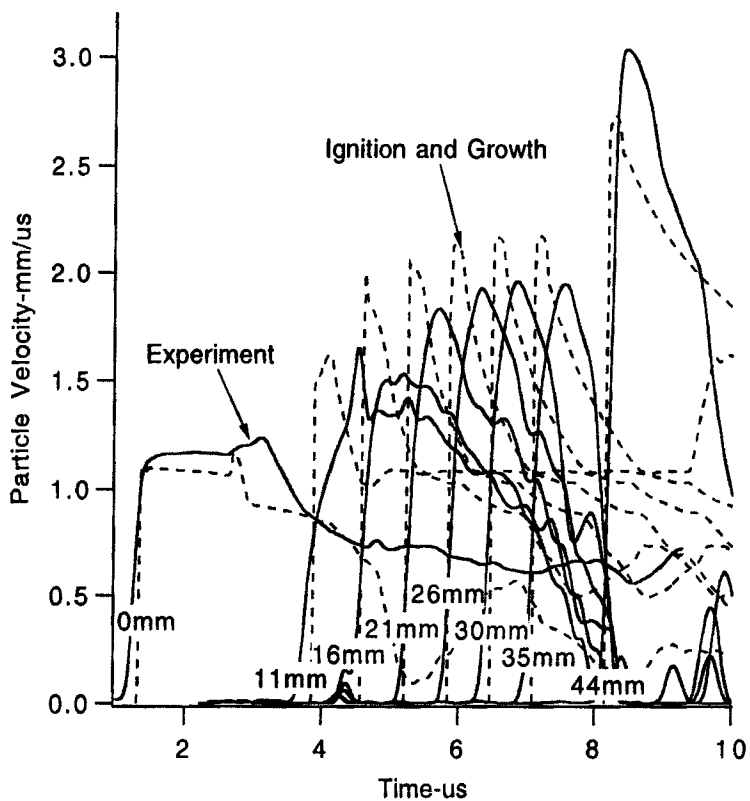


Figure 7. Experimental and Calculated Particle Velocity Histories in TATB/FEFO Impacted by an AD998 Flyer at 1.476 km/s



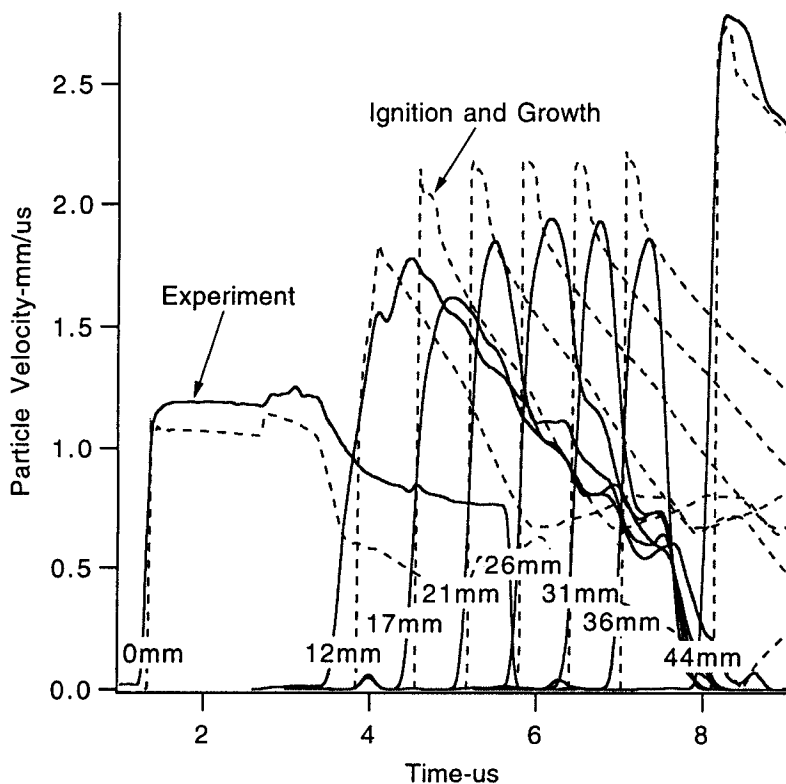


Figure 8. Experimental and Calculated Particle Velocity Histories in TATB/FEFO Impacted by an AD998 Flyer at 1.505 km/s

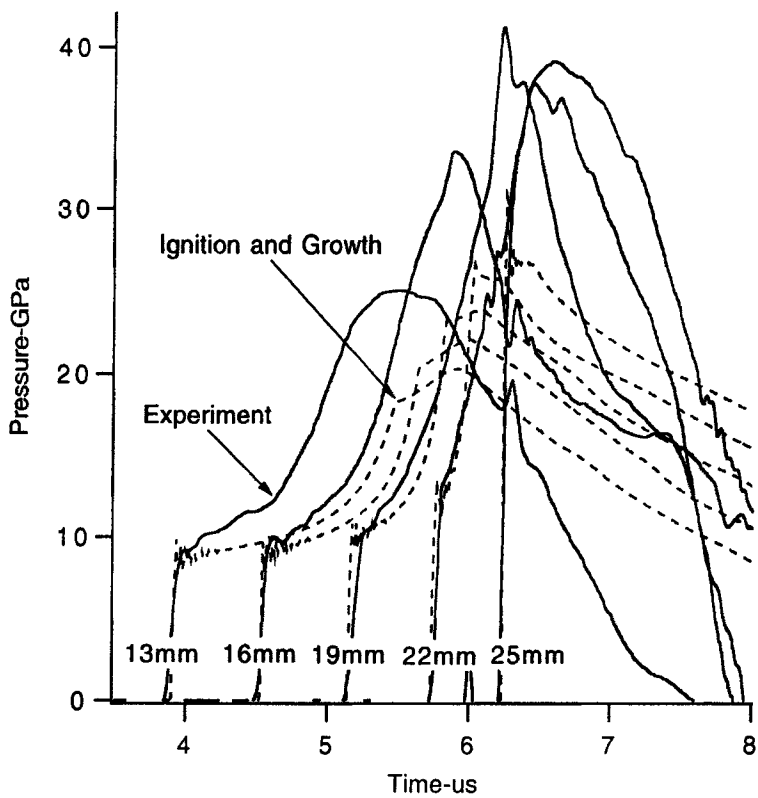


Figure 9. Experimental and Calculated Pressure Histories in TATB/FEFO Impacted by an Aluminum Flyer at 1.51 km/s

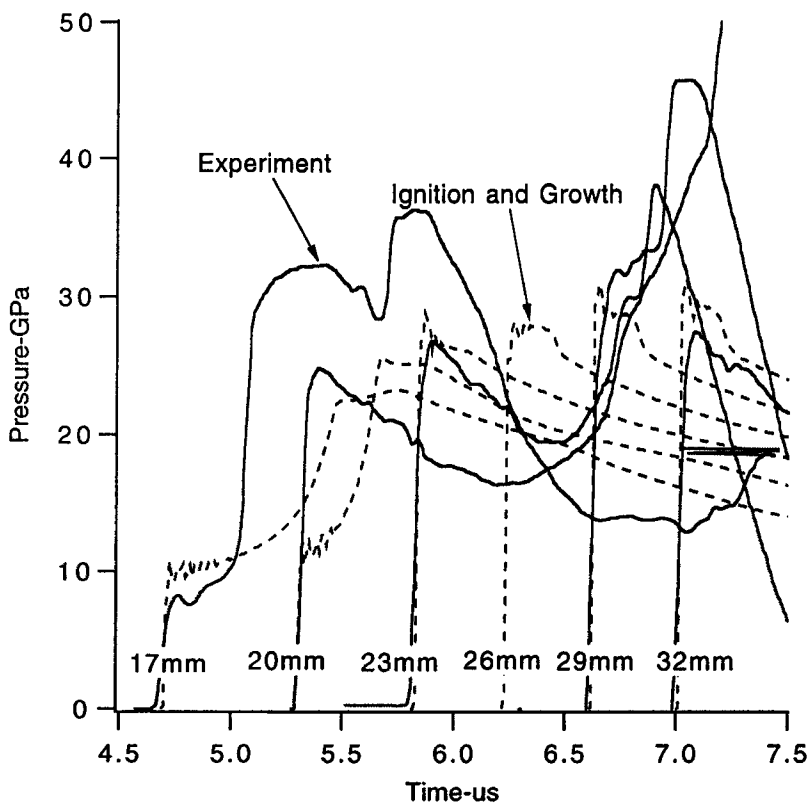


Figure 10. Experimental and Calculated Pressure Histories in TATB/FEFO Impacted by an Aluminum Flyer at 1.53 km/s

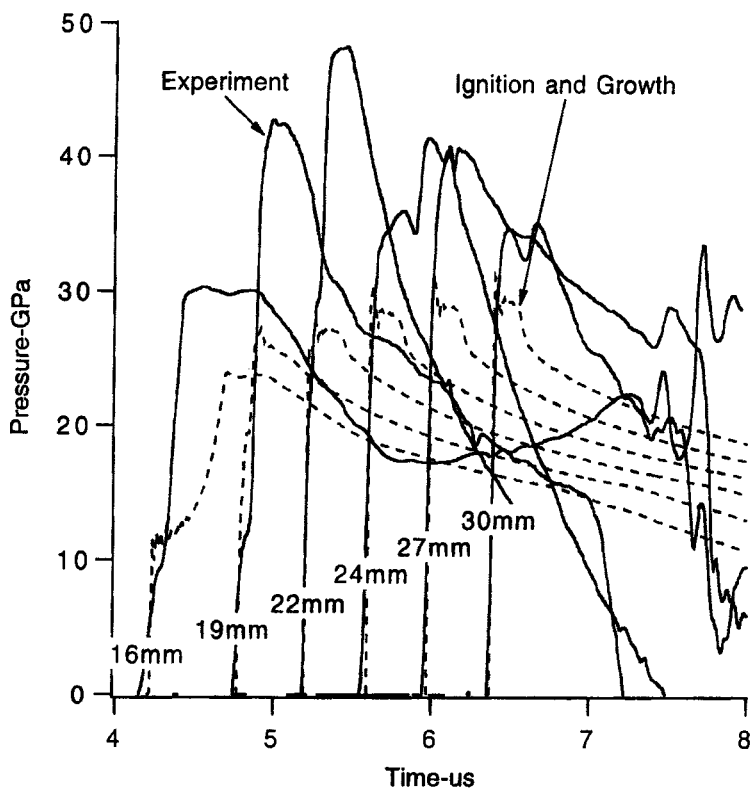


Figure 11. Experimental and Calculated Pressure Histories in TATB/FEFO Impacted by an Aluminum Flyer at 1.60 km/s

title 2d p gauges at fv=.1510 A=4e5(0.01) 6300p4 400p3  
 time= 2.97729E+00 contours of pressure  
 dsf = 1.00000E+00



min(-)=-1.000E-02  
 max(+)= 1.241E-01  
 contour levels

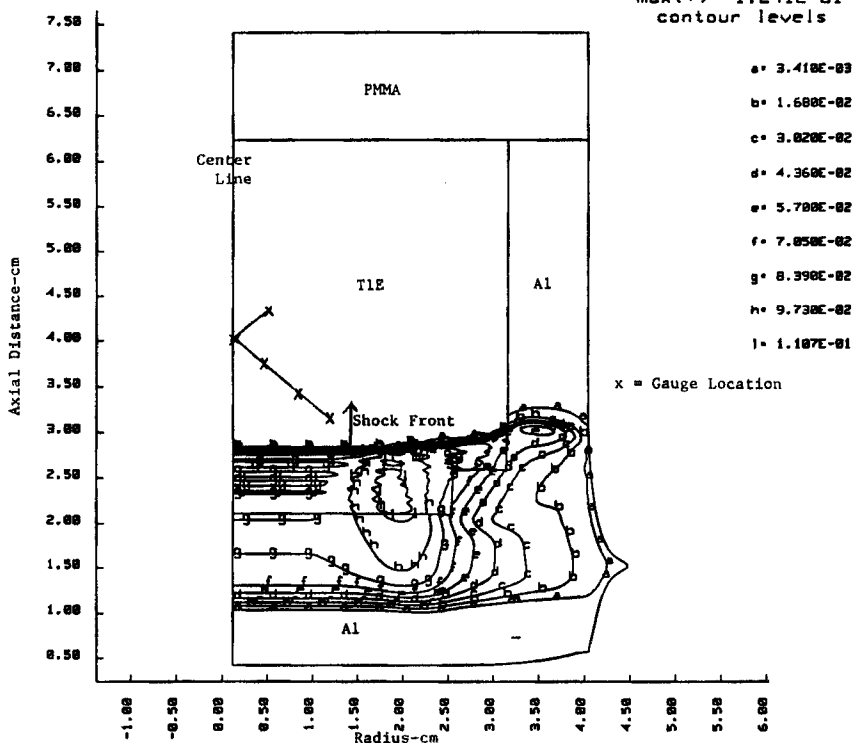



FIGURE 12

Pressure Contours in Aluminum and TIE at 3  $\mu$ s Following  
 Impact by an Aluminum Flyer at 1.51 km/s

title 2d p gauges at fv=1510 A=4e5(0.01) 6300p4 400p3  
 time= 3.93456E+00 contours of pressure  
 dsf = 1.00000E+00

  
 min(-)=-1.000E-02  
 max(+)= 1.982E-01  
 contour levels

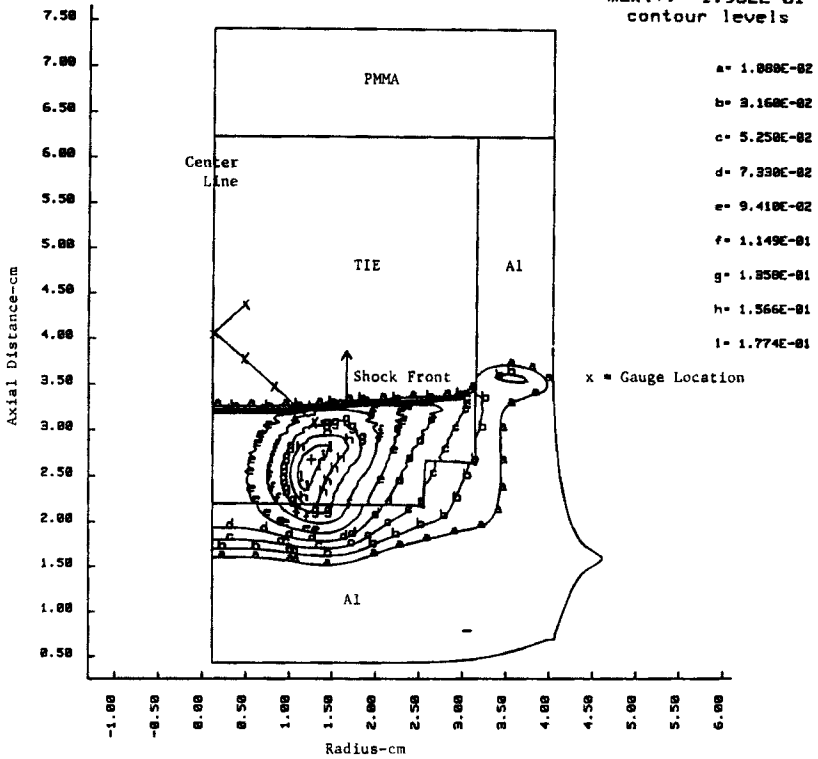


FIGURE 13

Pressure Contours in Aluminum and TIE at  $4 \mu\text{s}$  Following  
 Impact by an Aluminum Flyer at 1.51 km/s

tie 2d p gauges al fv= .1510 A=4e5(0.01) 6300p4 400p3  
 time= 4.94923E+00 contours of pressure  
 dsf = 1.00000E+00



min(-) = -1.000E-02  
 max(+) = 3.828E-01  
 contour levels

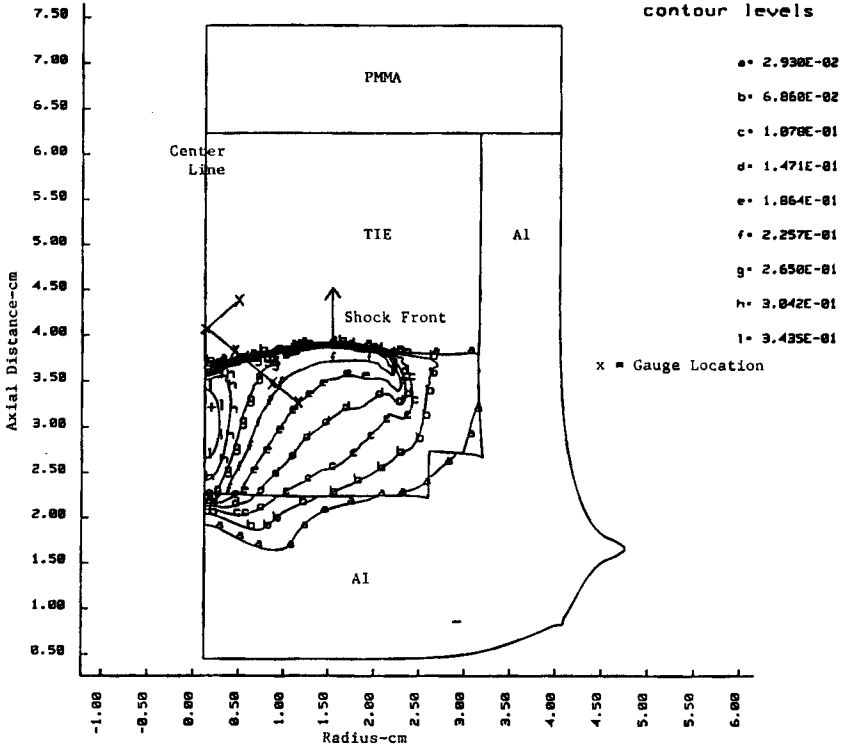


FIGURE 14

Pressure Contours in Aluminum and TIE at 5  $\mu$ s Following Impact by an Aluminum Flyer at 1.51 km/s

tie 2d p gauges al fv .1510 A=4e5(0.01) 6300p4 400p3  
 time = 5.94926E+00 contours of pressure  
 dsf = 1.00000E+00



min(-) = -1.000E-02  
 max(+) = 4.000E-01  
 contour levels

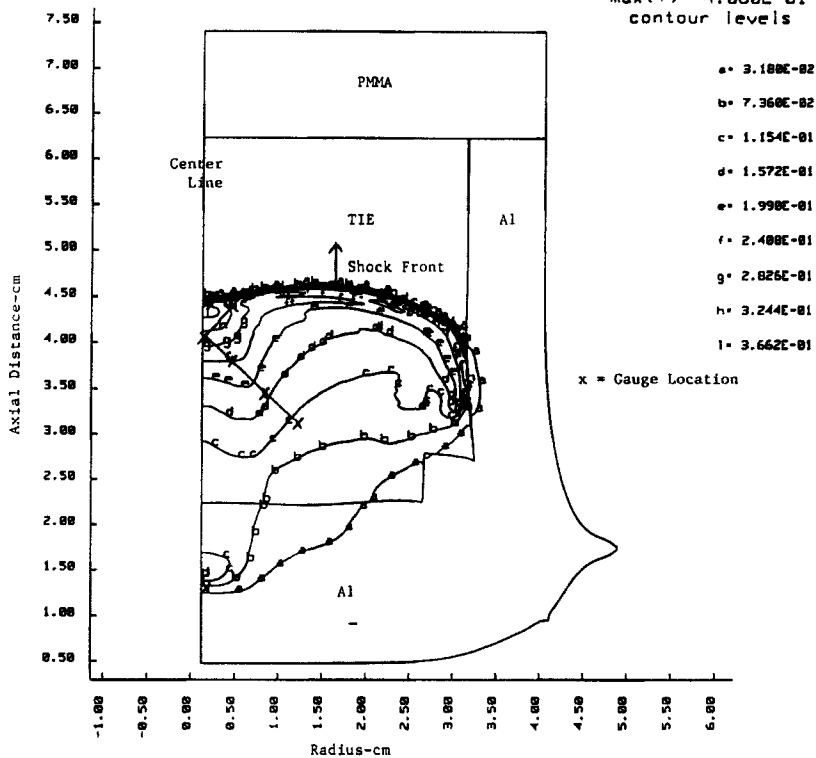


**FIGURE 15**  
 Pressure Contours in Aluminum and TIE at 6  $\mu$ s Following  
 Impact by an Aluminum Flyer at 1.51 km/s



the 2d p gauges at fv=1.510 A=4e5(0.01) 6300p4 400p3  
 time= 6.94471E+00 contours of pressure  
 dsf = 1.00000E+00

min(-)=-1.000E-02  
 max(+)= 3.890E-01  
 contour levels

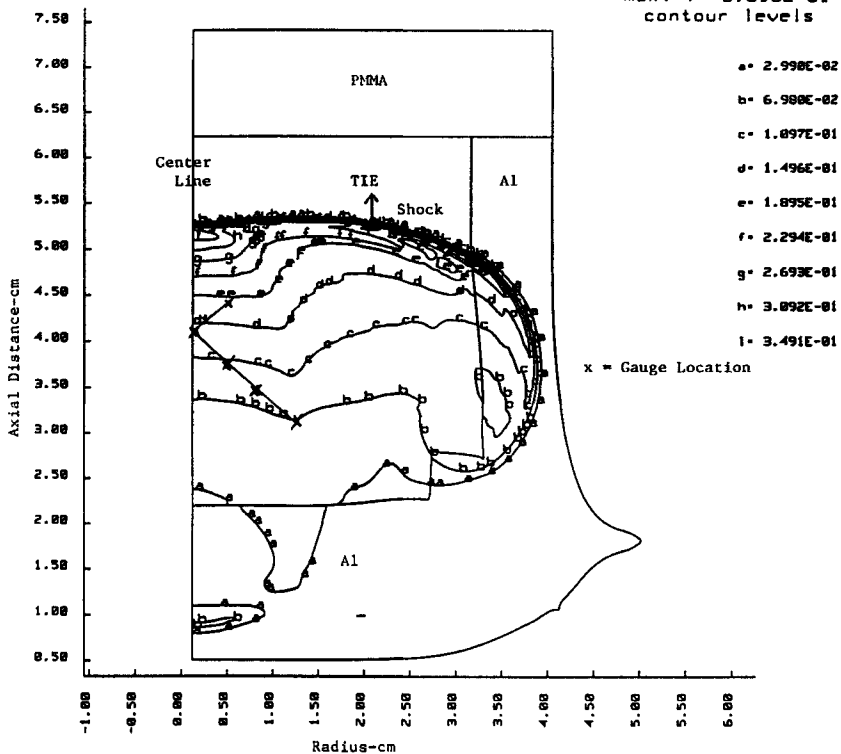


**FIGURE 16**  
 Pressure Contours in Aluminum and TIE at 7  $\mu$ s Following  
 Impact by an Aluminum Flyer at 1.51 km/s